



ELSEVIER

Coastal Engineering 46 (2002) 139–157

**Coastal
Engineering**
An International Journal for Coastal,
Harbour and Offshore Engineers

www.elsevier.com/locate/coastaleng

Unsteady air bubble entrainment and detrainment at a plunging breaker: dominant time scales and similarity of water level variations

Hubert Chanson^{a,*}, Shin-ichi Aoki^b, Mamoru Maruyama^b

^aDepartment of Civil Engineering, University of Queensland, Brisbane, QLD 4072, Australia

^bDepartment of Architecture and Civil Engineering, Toyohashi University of Technology, Toyohashi, 441-8580, Japan

Received 29 May 2001; received in revised form 6 March 2002; accepted 25 April 2002

Abstract

At plunging breakers, air bubbles are entrained at the impingement of the water jet, formed at the top of the wave, with the water free surface in front. During the present study, air bubble entrainment at a pseudo-plunging breaker was investigated at near full-scale and further experimental work studied the bubble detrainment process. Experimental observations included the generation and propagation of waves downstream of the plunge point. Experimental results highlighted a number of unsteady air–water flow patterns and emphasise high levels of aeration: i.e., depth-averaged void fraction of more than 10% next to jet impact in shallow waters. Unsteady bubble injection experiments showed a strong vortical motion induced by the rising bubbles. Altogether, the results suggest that a dominant time scale is the bubble rise time d_1/u_r , which cannot be scaled properly with an undistorted Froude model. The study contributes to a better understanding of unsteady bubble entrainment at a pseudo-plunging breaker and the associated vortical circulation. © 2002 Elsevier Science B.V. All rights reserved.

Keywords: Entrainment; Detrainment; Water level variations

1. Introduction

Air bubble entrainment by breaking waves is a significant factor in the surf zone under high wave conditions, in terms of water quality and energy dissipation. Air–water mass transfer across the air bubble interface is significant as the net surface area of thousands of tiny bubbles is much greater than the surface area above the bubble clouds (e.g., Daniil and Gulliver, 1991; Wallace and Wirick, 1992; Chanson

and Cummings, 1994). Recently, Aoki et al. (2000) proposed that air entrainment at plunging breakers may be one of the mechanisms of energy transfer from short waves to long-period waves near the shoreline. Long waves with periods of several minutes have been recognised as an important exciting component to beach erosion, sedimentation in harbours, harbour oscillations (seiching) and oscillations of moored ships in havens (e.g., Sawaragi, 1995; Komar, 1998).

With plunging breakers, the entrainment of air bubbles is caused by the top of the wave forming a water jet projecting ahead of the wave face and entraining air when it impacts the water free surface in front of the wave (e.g., Lin and Hwung, 1992;

* Corresponding author. Fax: +61-7-33-65-45-99.

E-mail address: h.chanson@mailbox.uq.edu.au (H. Chanson).

Chanson and Lee, 1997) (Fig. 1). In deep waters, plunging breaking waves may be caused by surface wind shear and constructive wave interference during high winds (e.g., Coles, 1967; Griffin, 1984; Longuet-Higgins, 1988). Such breakers have the ability to entrain a large number of bubbles at great depths

(e.g., Kanwisher, 1963; Kolovayev, 1976; Thorpe, 1982). In shallow waters, the air entrainment process and bubble residence time are affected by the sloping bottom, but bubble entrainment is still significant as highlighted by the “white water” pattern (Fig. 1B) (also Deane, 1997). The entrained bubbles induce a

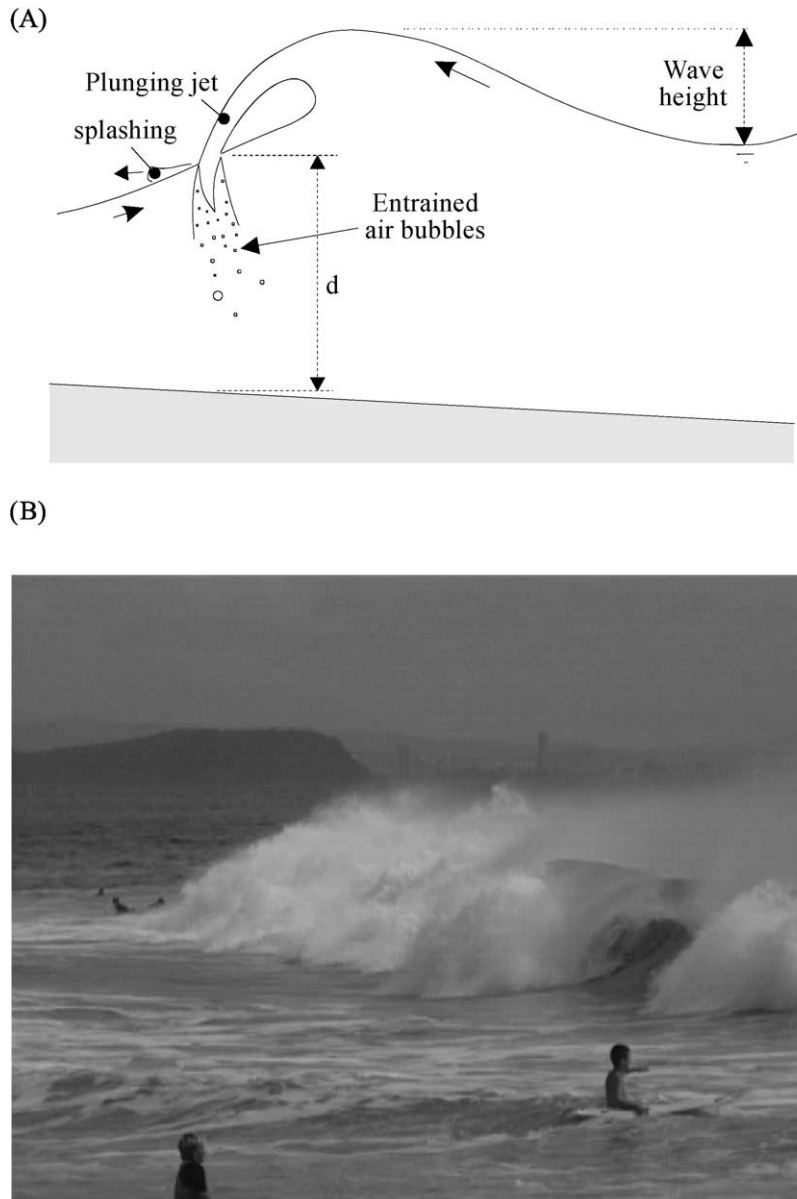


Fig. 1. Plunging breaking waves. (A) Sketch of a plunging breaker; (B) wave breaking near the shoreline on the Gold Coast, Rainbow Beach after 2 days of big swell (Easter 2001)—end of a plunging breaker with surfers in front, Rainbow Beach, Gold Coast.

rise in water level associated with an energy transfer into potential energy while breaker-generated waves propagate in off- and onshore directions (e.g., Fuhrbater, 1970; Hwung et al., 1992).

The influence of entrained air on the wave field near the surf zone has not yet been well investigated except for some research on energy dissipation by wave breaking. Since the air bubble entrainment process is not properly scaled by Froude's law, most laboratory experiments tend to underestimate its effects, particularly on the wave field (Wood, 1991; Chanson, 1997). In the present study, air bubble entrainment at a pseudo-plunging breaker was investigated at near full-scale. The pseudo-plunging breaker generated jet impact velocities ranging from 5.6 to 6.4 m/s. For comparison, the breaking wave height in Fig. 1B was about 2–3 m corresponding to an impact velocity of about 6–7 m/s. The work is focused on the unsteady flow patterns associated with air entrainment and detrainment, as well as the dominant time scales. The results provide new information on the unsteady plunging jet process, the rise in free-surface level caused by air entrainment, the effect on the wave field and the similarity of water level variations.

2. Physical modelling of a plunging breaker

In a physical model, the flow conditions are said to be similar to those in the prototype if the model

displays similarity of form, similarity of motion and similarity of forces. For wave motion studies, the gravity effect is usually predominant, and model–prototype similarity is performed with a Froude similitude. If the same fluids are used in both model and prototype, distortions are introduced by effects other than gravity (e.g., viscosity, surface tension) resulting in scale effects.

Considering a single plunging breaker, the characteristic time scale of the initial air entrainment equals d_1/V_1 , where d_1 is the initial water depth and the jet impact velocity V_1 is basically proportional to the square root of the wave height (e.g., Chanson and Lee, 1997). A further time scale is the breaker duration t_{jet} that is a function of the breaker volume per unit width. The characteristic time scale of air detrainment is the bubble rise time d_1/u_r , where u_r is the bubble rise velocity.

Both in the field and in the laboratory, entrained bubbles are about millimetric and the rise velocity is nearly constant for bubble diameters ranging from 0.5 to 50 mm (Wood, 1991; Chanson, 1997). As a result, the scale ratio of the characteristic air detrainment time becomes:

$$\left(\frac{d_1}{u_r}\right)_R = L_R \quad (1)$$

where the subscript R denotes the ratio of prototype-to-model quantity and L_R is the geometric scaling ratio. However, a Froude model implies that the

Table 1
Summary of experimental flow conditions

| Experiment | Initial tank volume (m ³) | Initial head above orifice H_1 (m) | Fall height orifice-bed (m) | Initial flume conditions | Initial flow rate $Q(t=0+)$ (m ³ /s) | Remarks |
|------------|---------------------------------------|--------------------------------------|-----------------------------|--|---|--|
| Series 1 | | | | | | |
| 1A | 0.42–1.2 | 0.31–0.78 | 1.324 | $d_1 = 0.2\text{--}0.47$ m, $B = 0.8$ m | 0.08–0.13 | Free-falling jet, 33 experiments |
| 1B | 0.42–1.2 | 0.31–0.77 | 1.324 | $d_1 = 0.2\text{--}0.47$ m $B = 0.8$ m | 0.10–0.16 | Plastic cellophane sheets to suppress air entrainment, 20 experiments |
| Series 2 | | | | | | |
| | N/A | N/A | N/A | $d_1 = 0.50$ m $B = 0.05$ m | N/A | Bottom injection of air (37.3 l/min), 17 experiments |
| 2-1 | | | | No air injection | | Sudden air injection ($t > 0$) |
| 2-2 | | | | Continuous air injection | | Sudden end of air injection ($t > 0$) |
| 2-3 | | | | No air injection | | Controlled air injection for $0 < t < t_{\text{inj}}$ with $1 \text{ s} \leq t_{\text{inj}} \leq 20 \text{ s}$ |

B : channel width; d_1 : initial flume water depth; H_1 : initial head in the reservoir; freshwater experiments.

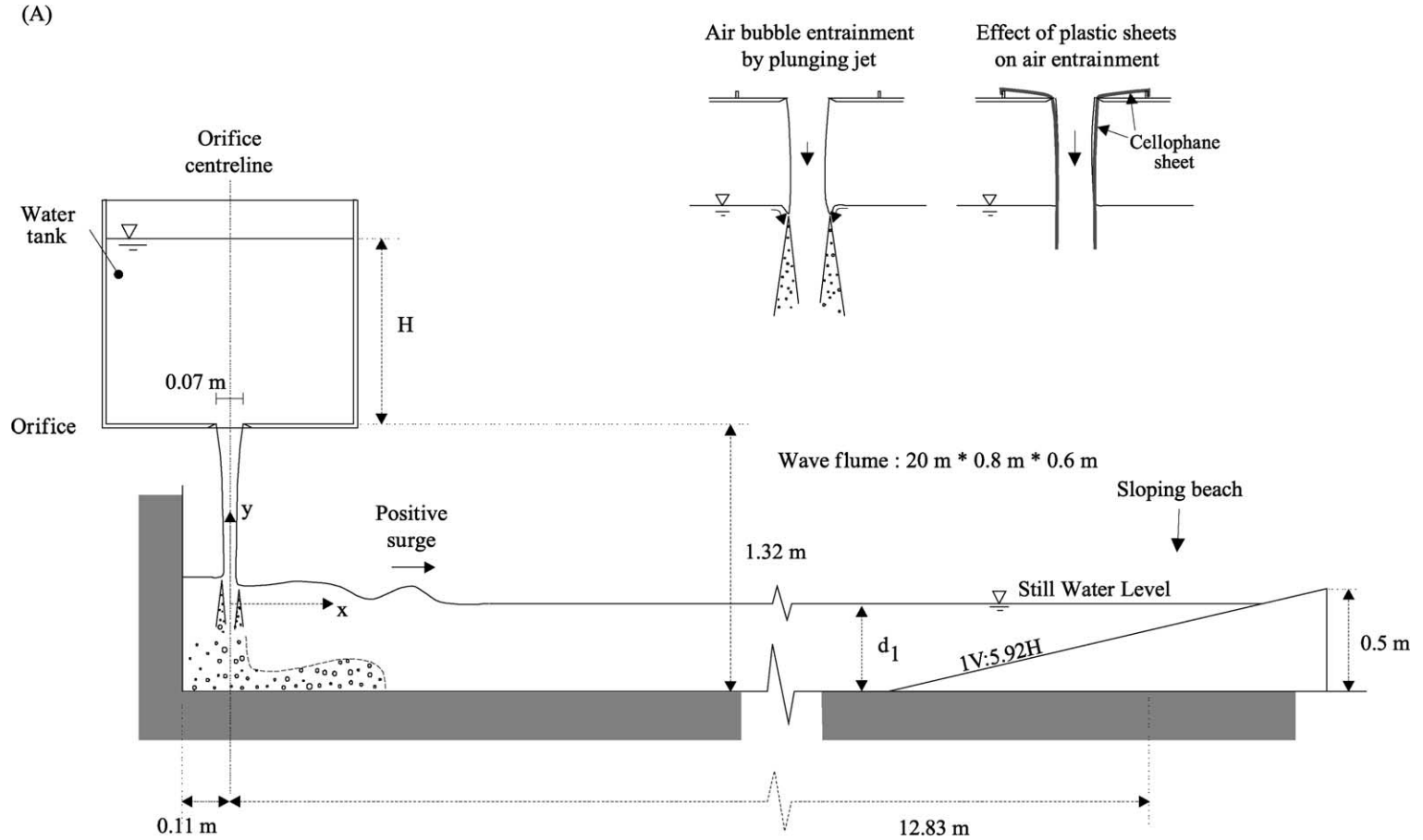


Fig. 2. Experimental facilities. (A) First experimental facility; (B) second experimental facility.

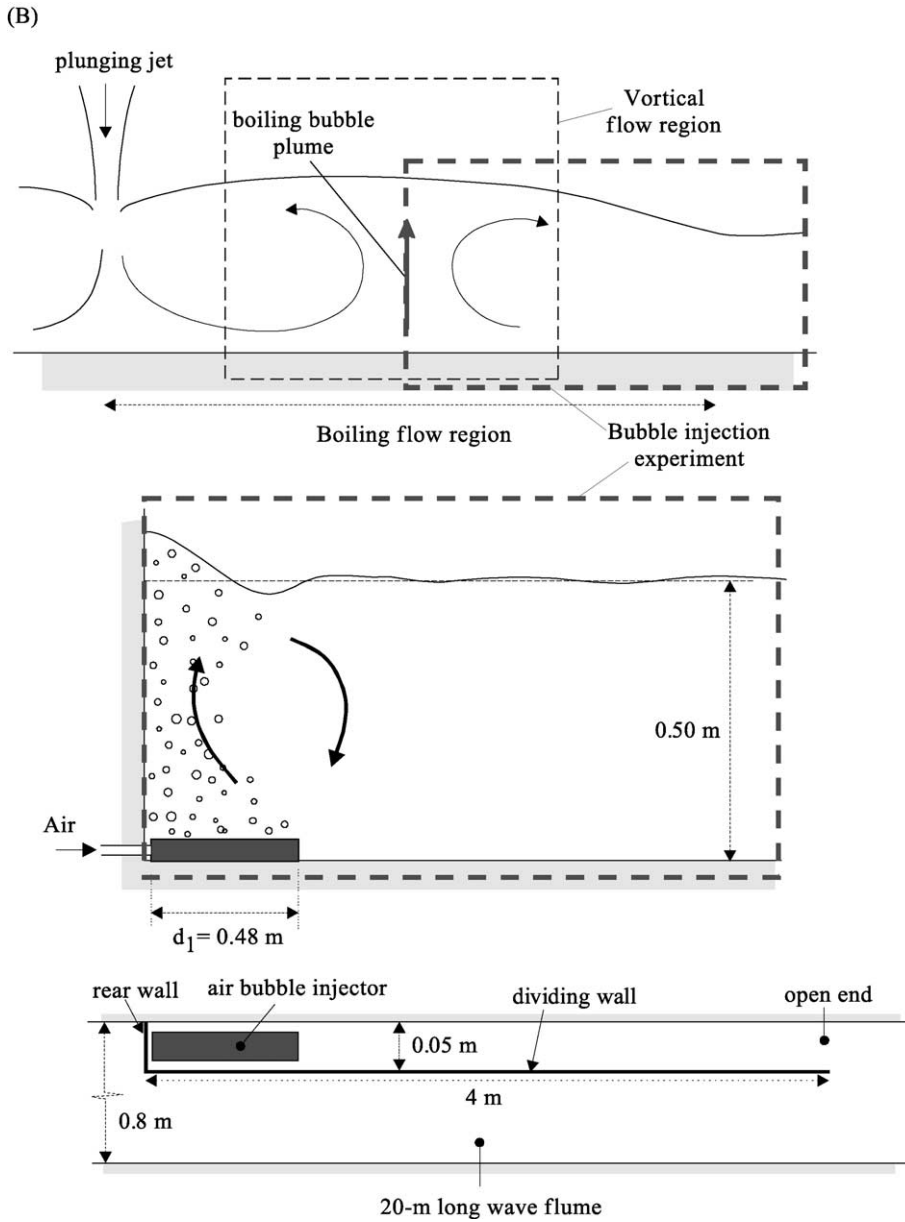


Fig. 2 (continued).

characteristic times must be scaled by $\sqrt{L_R}$ (e.g., Ippen, 1966; Hughes, 1993; Chanson, 1999). Eq. (1) demonstrates that the bubble rise time increases with the water depth and cannot be scaled with a Froude similitude.

Numerous experimental studies of air entrainment by plunging jets showed that the volume of entrained air per meter width may be estimated as:

$$q_{\text{air}} \propto (V_1 - V_c)^N \quad (2)$$

where V_e is the onset velocity for air bubble entrainment, and the exponent N is about 3 for low jet velocities and equals to 2 for high jet velocities (reviews by Wood, 1991; Bin, 1993; Chanson, 1997). In freshwater, the onset velocity V_e is about 1–3.5 m/s (Cummings and Chanson, 1999). Eq. (2) implies that a Froude similitude cannot scale properly the volume of entrained air by using the same fluids in model and prototype (unless $V_e=0$ and $N=1$). Small-sized models basically underestimate the air entrainment, and sometimes, no air entrainment is observed when the plunging jet velocity is smaller than the onset velocity V_e .

A further important time scale is the period of the wave group. Larger wave heights are associated with stronger air entrainment than smaller waves. The rise of water level caused by bubble entrainment will be more significant in the bulge of the group envelope. As a result, this effect may generate water level oscillations with a period equal to that of the wave group.

Considering a plunging breaker near the shoreline, the jet flow and the associated boiling flow pattern contribute to set sediment matters into suspension. The strong turbulent mixing, observed in the laboratory and in the field, is further enhanced by the upwelling circulation induced by the rising air bubbles. Subsequently, the combined effects of jet mixing and rising bubbles have a direct impact on the sediment transport processes (e.g., Nielsen, 1984). Physical modelling of the three-phase flow is practically impossible, but at full-scale.

3. Experimental setup

Two series of experiments were conducted with freshwater (Table 1, Fig. 2). The first one was focused on the unsteady plunging jet process, the associated air bubble entrainment and detrainment. A strong boiling flow process was observed (Section 4). The second experiment was designed to investigate spe-

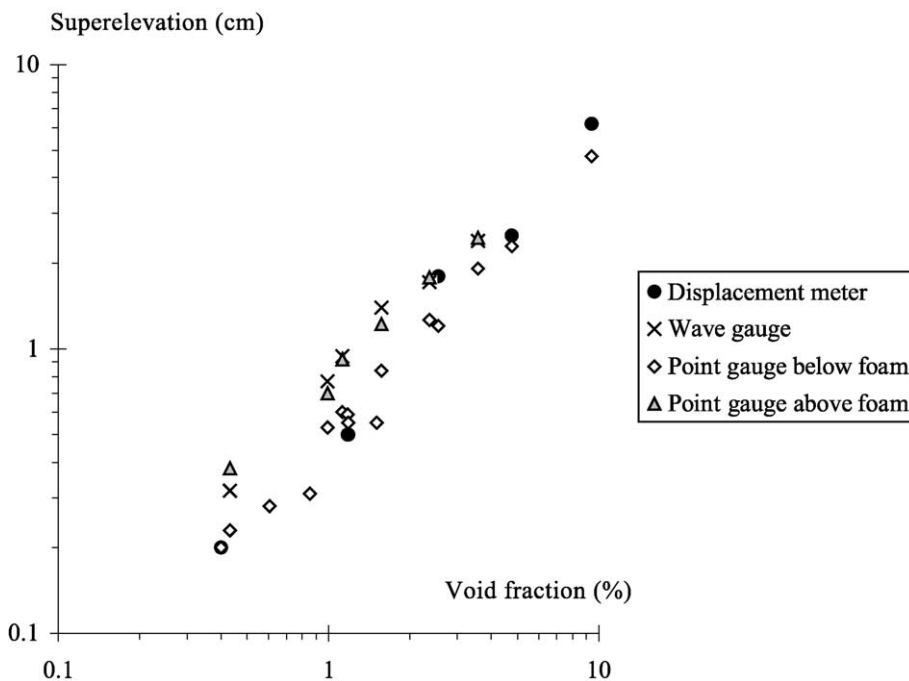


Fig. 3. Accuracy of capacitance water gauge and displacement meter in bubbly waters: superelevation (or water level rise above still water) as a function of the depth-averaged void fraction.

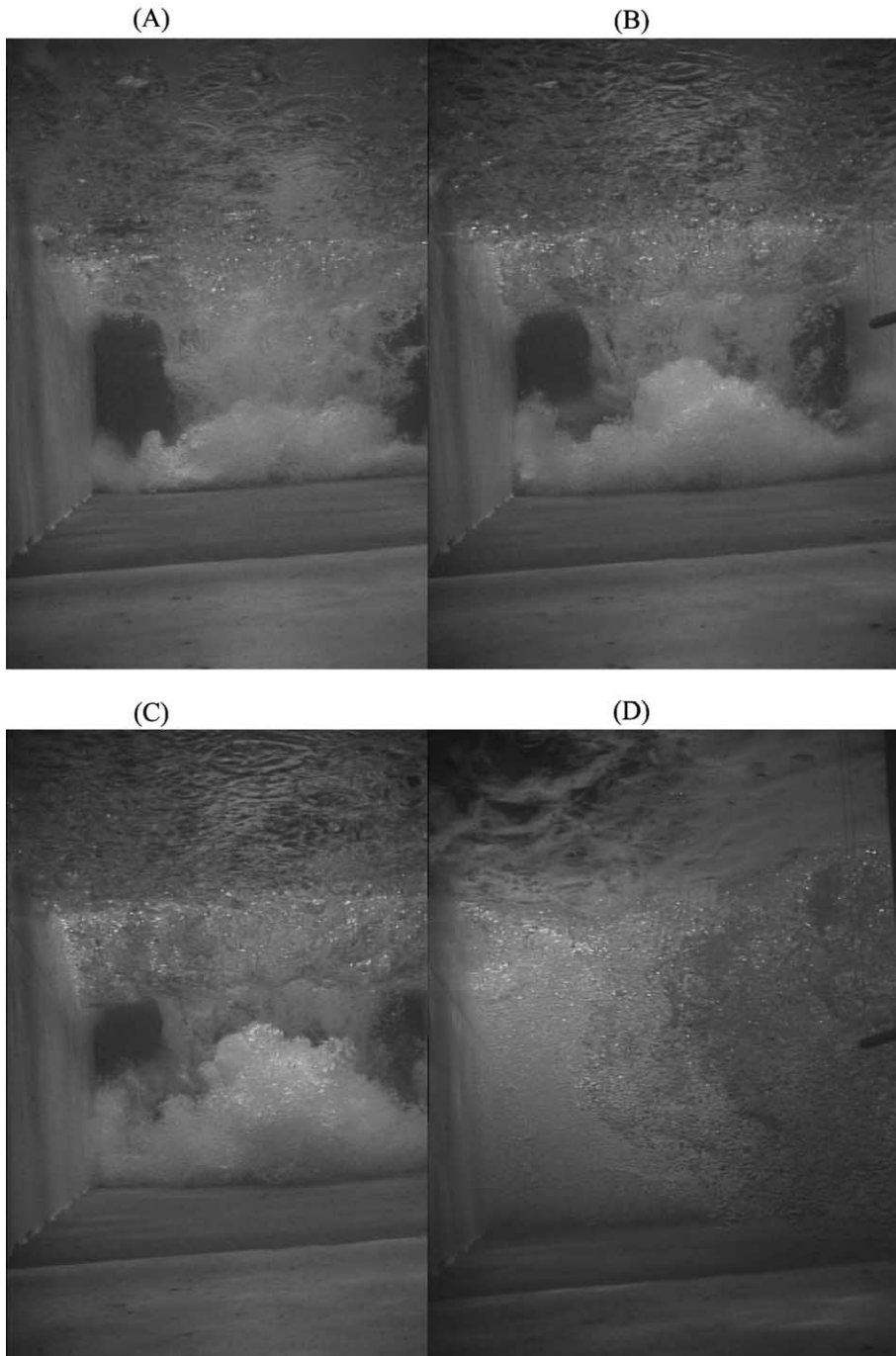


Fig. 4. Underwater photographs of the bubbly plume—initial water volume: 0.628 m^3 , $d_1 = 0.35 \text{ m}$. Camera located at $x \approx 2 \text{ m}$, looking toward the nappe impact. (A) $t = 11/30 \text{ s}$; (B) $t = 14/30 \text{ s}$; (C) $t = 16/30 \text{ s}$; (D) $t = 40/30 \text{ s}$.

cifically the boiling phenomenon and the effects of rising bubbles on the flow field (Fig. 2B).

In the first series of experiments (Series 1), the plunging jet of the breaker was modelled by an unsteady vertical jet discharging into a 20-m-long, 0.8-m-wide, 0.6-m-deep flume. The pseudo-plunging breaker was generated by a known volume of water ($0.4\text{--}1.2\text{ m}^3$) discharging through a rectangular sharp orifice ($0.75 \times 0.07\text{ m}$) located 1.32 m above the flume invert. A sloping beach ($1V:6H$) was installed at the end of the working section (Fig. 2A). The orifice was closed by a steel gate prior to each experiment. The gate release occurred in less than 0.030 s and the free-falling nappe took less than 0.3 s to reach the water surface. The duration of the pseudo-plunging breaker ranged from about 5 to 12 s depending upon the initial water volume (Table 1). For some experiments, air entrainment was reduced by a factor of 2–3 by inserting 18- μm plastic films which were fixed inside the water tank, covered the nappe and inhibited bubble entrainment at the plunge point. The cellophane sheet surrounded the free-falling nappe like stockings. Tests showed that the cellophane sheet did not affect the falling jet. Its weight was negligible and insignificant compared to the jet momentum.

In a second series of experiments (Series 2), the process of water level rises due to air entrainment, and the effects of air detrainment were idealised by an air bubble generator (0.48 m long, $\varnothing = 0.045\text{ m}$, air discharge up to 0.62 l/s) installed at the bottom of a 4-m-long, 0.05-m-wide section of the wave flume. The air bubble generator was located next to a rear wall and discharged air bubbles into still water with a known depth ($d_1 = 0.5\text{ m}$) (Fig. 2B) (the air flow rate was 0.62 l/s for all experiments). The other end of the test section was open to the wave flume. The configuration was somehow similar to half of a pneumatic breaker (e.g., Straub et al., 1959), but the emphasis was put here on unsteady air injections (the rear wall acted as a symmetry line, hence, only half of a rising cloud was simulated). Basic experiments included sudden air injection, sudden end to bubble injection and air injection for a controlled duration, with bubble injection periods ranging from 1 to 20 s. Water level fluctuations were measured at several locations along the flume.

3.1. Instrumentation

Flow visualisations, nappe trajectory, impact flow conditions and underwater bubble plume were inves-

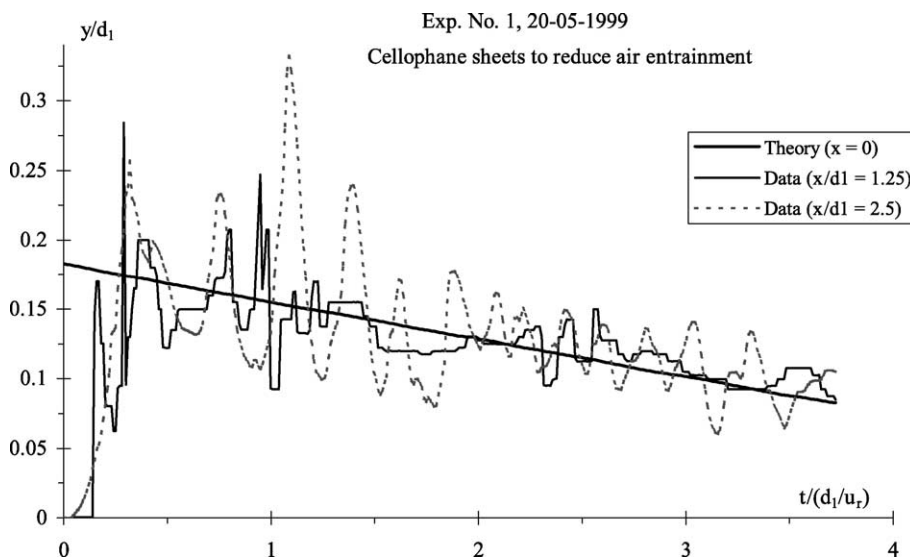


Fig. 5. Comparison between observed water elevations and theoretical solution of the bore and negative surge at the origin. $H_1 = 0.571\text{ m}$, $d_1 = 0.40\text{ m}$, $u_r = 0.2\text{ m/s}$, Exp. No. 990520_1 with cellophane sheets to reduce air entrainment.

tigated with two video cameras: a VHS-C camcorder National™ CCD AG-30C (speed: 30 frames/s, shutter: 1/60 and 1/1000 s) and a digital handycam Sony™ DV-CCD DCR-TRV900 (speed: 30 frames/s, shutter: 1/4–1/10,000 s, zoom: 1–48).

Water depths in the reservoir and in the flumes were measured with pointer gauges, capacitance wave gauges and displacement meter. The wave gauges were Kenek™ capacitance gauges with a 10-Hz response and an accuracy of about 1 mm (tested during on-site calibration). One ultrasonic displacement meter Keyence™ UD300 was also used (range: 0.20–1.30 m, response: 10 Hz, accuracy: 1 mm, $\varnothing = 20$ mm). The probes were scanned at 50 Hz for 163.8 s.

The effect of air bubbles on wave gauge and displacement meter readings was tested in a preliminary experiment. Air was introduced at the bottom end of a vertical cylinder installed in a still water tank. Tests, performed with void fractions ranging from 0 to 0.10, showed that both wave gauges and displacement meter recorded with a reasonable accuracy the rise in water level induced by the air bubbles. The error was of the same order of magnitude as the bubbly foam thickness formed at the water surface in the cylinder, although the output of the gauge tended to correspond to the level above the foam (Fig. 3). Fig. 3 presents measured superelevations above still water as functions of the depth-average void fraction for comparable tests.

In the plunging jet experiment (Series 1), the time origin ($t=0$) was taken at the instant when the nappe impacted onto the water free surface. The time t was nondimensionalised in terms of the bubble rise time that was found to be a dominant time scale: i.e., $T=t/(d_1/u_r)$, u_r being the bubble rise velocity in still water. The u_r was the speed of the most frequent bubbles. Distances and depths were nondimensionalised in terms of the initial water depth: e.g., $X=x/d_1$. The longitudinal origin ($x=0$) was at the centreline of the vertical nappe (Fig. 2). The instantaneous orifice flow rate was deduced from the water level measurements in the tank. The relationship between water height and water volume was calibrated in situ with a container of known volume.

A number of verifications were performed to ensure the repeatability and consistency of the experiments. Further details were reported in Chanson et al. (1999) and Maruyama (2000).

4. Unsteady flow patterns

4.1. Pseudo-plunging breaker

The initial impact was associated with a strong splashing of short duration (i.e., less than 0.4 s) and the generation of a downward underwater bubble plume. The splashing was characterised by very small liquid fractions (i.e., less than 2%), and some droplets would travel up to 2.5 m from the impact point and reach heights in excess of 0.4 m above the initial free-surface level. A similar splashing process was observed during the initial stage of the plunging breaking wave in the laboratory (e.g., Perlin et al., 1996; Tulin and Waseda, 1999).

The initial bubble entrainment was a densely populated bubble plume travelling downwards. The bubble plume took about 0.23–0.27 s (i.e., $T=0.065–0.135$) to reach the channel bottom for a 0.4-m water depth with an impact velocity of about 5.8–6.1 m/s. As the bubble plume reached the bed, a stagnation point developed and the plume was deflected horizontally (Fig. 2A). A bubbly turbidity current flowed parallel to the bed with clear water above and the plume front expanded as some bubbles rise (Fig. 4). Fig. 4 shows a series of underwater photographs taken during one experiment. The camera was located at $x \approx 2$ m looking at the bubble plume progression. On the last photograph, the rising bubbles almost reached the free surface. The horizontal bubbly flow ran for a distance of about $x=1–1.2$ m ($X \sim 2.5–5$) before most bubbles rise to the free surface by buoyancy. Slow-motion pictures suggested that the celerity of the bubble plume front was about 30–45% of the jet impact velocity V_1 , although the plunging jet flow was not fully developed at stagnation.

This rapid sequence of events was followed by the development of a “boiling” flow pattern next to the plunge point. This flow region was extremely turbulent with a large amount of entrained air bubbles, having the same appearance as a hydraulic jump roller. The “roller” region occupied a large surface area: i.e., $x \leq 1.5–2$ m ($X \leq 3–5$). The boiling flow pattern lasted typically 3–7 s (i.e., $\Delta T=3–7$) longer than the free-falling nappe (i.e., pseudo-plunging breaker). Bubbles were still observed under water after the disappearance of the boiling flow. Visually, most entrained air bubbles disappeared around $t=25–$

40 s (i.e., $T=15-25$). A time delay, between the end of pseudo-plunging breaker and end of the boiling flow pattern, was observed for all experiments.

Shortly after jet impact, a positive surge propagated into the flume. It was followed by a negative surge corresponding to a reduction in the orifice flow rate (e.g., Henderson, 1966; Montes, 1998). When air entrainment was suppressed, the free-surface levels measured at several locations along the flume were in close agreement with theoretical results deduced from the continuity and momentum principles for the bore front and from the equations of Saint-Venant for negative surge (Fig. 5). Fig. 5 presents dimensionless water levels y/d_1 as functions of the dimensionless time $T=t/(d_1/u_r)$, where y is the water elevation measured above the (initial) still water level. A value of $u_r=0.2$ m/s was observed and it is characteristic of the observed millimetric bubbles (e.g., Comolet, 1979; Chanson, 1997). Such a value is used thereafter.

4.2. Unsteady bottom injection of bubbles

In the second series of experiments, air injection generated an immediate water level rise above the injector that propagated subsequently in the flume (Figs. 6 and 7). Fig. 6 shows a photograph of the experiment (Fig. 6A), a sketch of the characteristic stages (Fig. 6B) and time variations of the free-surface profile next to the origin during one experiment (Fig. 6C). Fig. 7 presents time variations of water levels at several longitudinal positions with increasing bubble injection times from Fig. 7A–C (note that Fig. 7A–C have different horizontal scales).

The results showed a strong effect of the bubble injection time onto the water level fluctuations. For long bubble discharges (i.e., $T_{inj}>3$), the water level fluctuations were typically categorised into three stages, sketched in Fig. 6B and shown in Fig. 7. In Stage 1 ($0 \leq T \leq 1-2$), the water level rose as a direct result of air injection (Figs. 6A and 7 for $X=0.68$).

(A)



Fig. 6. Free-surface levels in the air injection experiment (Series 2). (A) Photograph taken at $t=3$ s ($t_{inj}=20$ s, $d_1=0.5$ m); (B) sketch of free-surface flow pattern next to the injection point; (C) dimensionless free-surface elevations Y (measured above still water level) next to the origin after air bubble injection ($T_{inj}>8$).

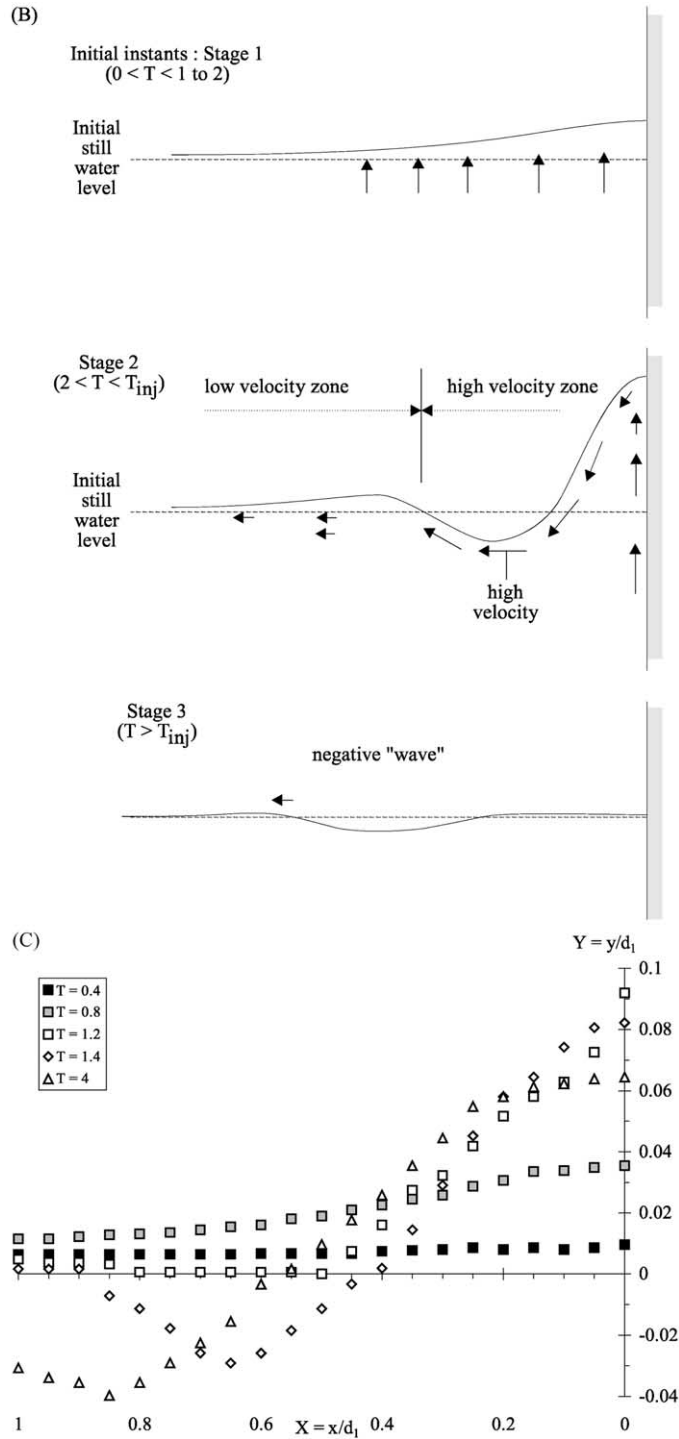


Fig. 6 (continued).

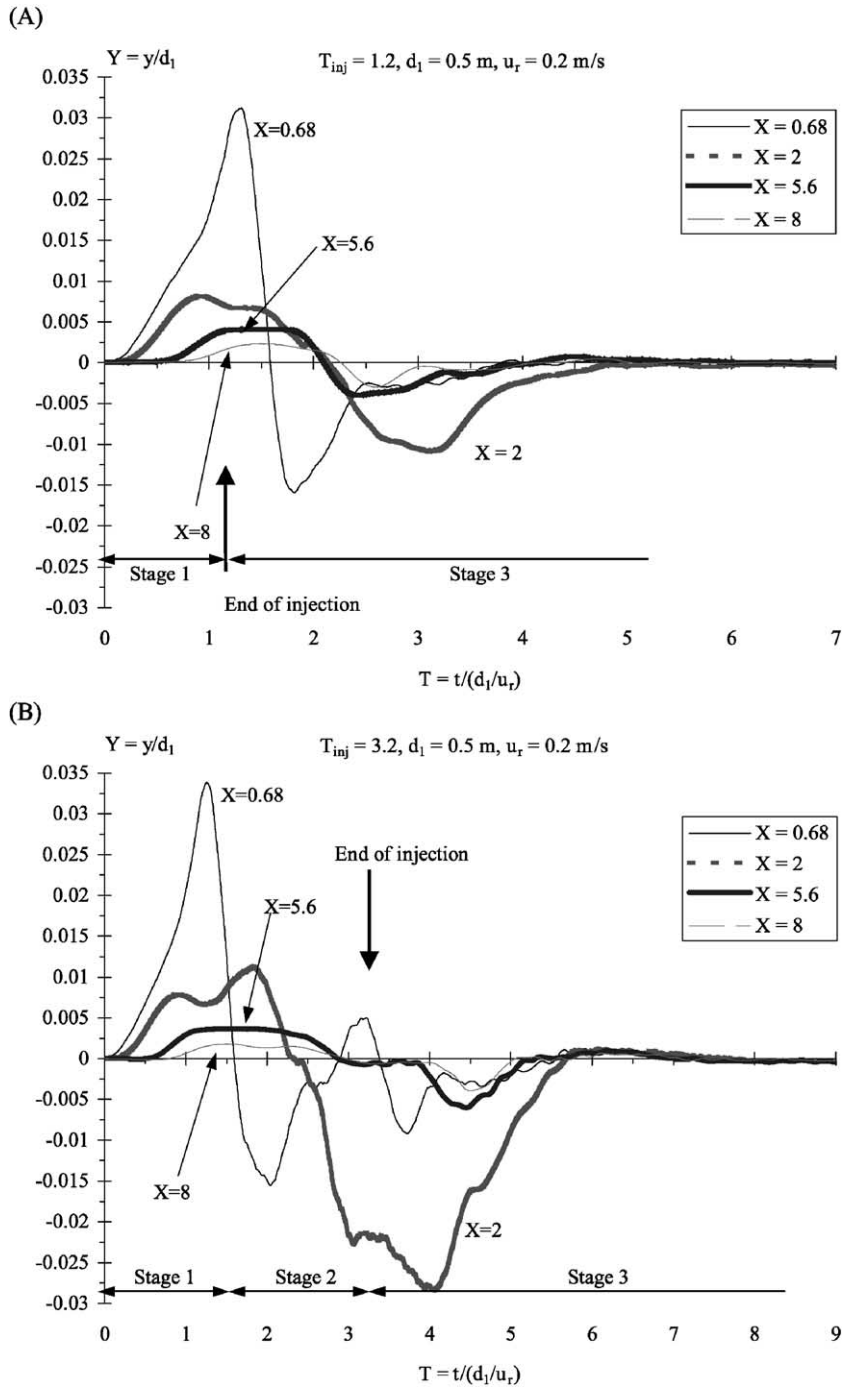


Fig. 7. Time variations of dimensionless water levels (above still water) y/d_1 for different bubble injection times. (A) $T_{inj} = 1.2$; (B) $T_{inj} = 3.2$; (C) $T_{inj} = 8.0$.

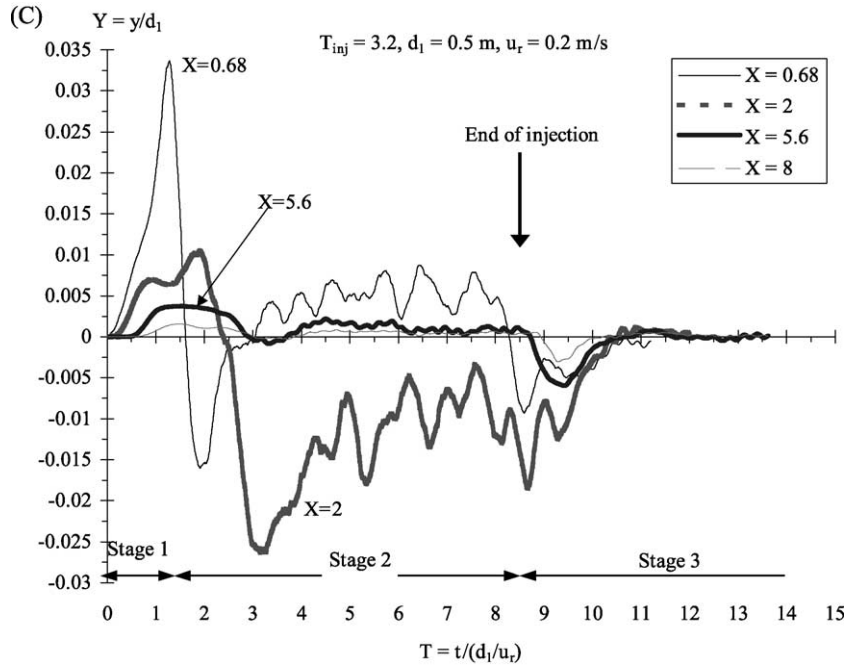


Fig. 7 (continued).

The characteristic time scale seemed to be a function of bubble rising time d_1/u_r . At the origin ($x=0$), the water level rise reached an equilibrium for $T \sim 1.4$. The water superlevation, measured above still water level, was the addition of flow bulking caused by air injection (i.e., $Cd/(1-C)$) and stagnation pressure resulting from the upward bubbly plume velocity w (i.e., $w^2/(2g)$). The water level rise propagated in the channel. The propagation speed, measured away from the injector ($x \geq 1$ m, $X \geq 2$), was about 2–2.4 m/s that is close to the celerity of a small disturbance $\sqrt{gd_1}$. The maximum water height measured above still water level seemed to decay hyperbolically with the distance. The dimensionless data were best correlated by

$$Y_{21\max} = \frac{8.30 \times 10^{-2}}{(X + 0.954)^{1.687}} \quad 0 < X < 9 \quad (3)$$

where $Y_{21\max}$ is the dimensionless water level rise (above still water), $Y=y/d_1$ and $X=x/d_1$.

In Stage 2 ($2 < T \leq T_{inj}$), a strong vortical circulation with large horizontal velocity component was

induced by the vertical upward current generated by the bubble plume. This generated a quasi-steady water level fall near the bubble generator and an associated water level rise at some distance. The horizontal velocity current and water level fall are sketched in Fig. 6B middle. The water level fall is also seen in Fig. 7B and C for $X=2$ with a trough at $Y=-2.75$. Video analysis, using air bubbles as tracers, highlighted a region of high velocity next to the trough (water level fall) while the velocities were significantly smaller further downstream.

The Stage 3 took place after switching-off the bubble generator (i.e., $T > T_{inj}$). The water level dropped following the propagation of the water level fall initially created near the bubble generator. A negative surge (i.e., a decrease in water level below the still water level) was observed propagating with an average celerity of about 2 m/s (the negative “wave” is sketched in Fig. 6B bottom). The maximum amplitude of the negative surge occurred at about:

$$T_{22} = T_{inj} + 1.05(1.28 - \exp(-0.51X)) \quad 0.6 < X < 9 \quad (4)$$

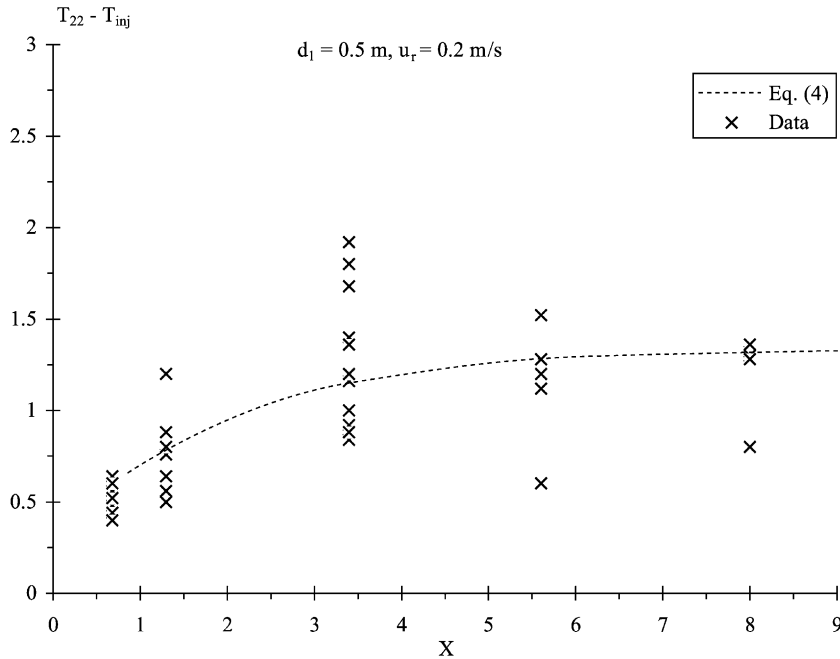


Fig. 8. Dimensionless time T_{22} at which the maximum negative surge amplitude was observed. Comparison between experimental observations and Eq. (4).

where $T = t/(d_1/u_r)$. Experimental data and Eq. (4) are compared in Fig. 8. The maximum amplitude of the “negative wave” decayed exponentially with distance and the data may be correlated by:

$$Y_{22\max} = -2.63 \times 10^{-3} \exp(-0.128X) - 7.24 \times 10^{-4} \quad (5)$$

$0.6 < X < 9$

Eqs. (4) and (5) were validated for finite injection times satisfying $T_{inj} \geq 0.4$. Overall, the water level variations caused by air bubble injection lasted consistently longer than the injection time. The total duration of water level variations was best correlated by:

$$T_{23\max} = 18.4(1.11 - \exp(-0.062T_{inj})) \quad (6)$$

$0.6 \leq T_{inj}$

corresponding to a time delay between the air injection end and the end of significant water level fluctuations of about: $T_{23\max} - T_{inj} \sim 2-2.5$.

For short injection periods ($T_{inj} < 3$), Stage 2 was sometimes eliminated as illustrated in Fig. 7A.

4.3. Discussion

The results of the Series 2 experiments highlight the strong scale vortical circulation generated by the rising bubbles and air detrainment (Figs. 2 and 6). This process took place also during experiments Series 1, although it could not be observed in such details.

The characteristic time scales of water level changes seemed to be strongly correlated to the bubble rise time d_1/u_r . As the bubble rise velocity is nearly identical in both experiments and actual wave field, the result implies that the water depth must be scaled 1:1. That is, the water depth must be the same in the field and in the laboratory.

5. Discussion

5.1. Effects of air entrainment

With free-falling jets and air bubble entrainment, a significant flow bulking (i.e., water level rise) was

observed next to the impact zone. It was generated by an upward displacement of water resulting from air entrainment. For all experiments with free jets, the water level data were consistently higher than theoretical predictions. The differences imply a depth-averaged void fraction of nearly 12% next to the impact zone and about 4–6% at about $X=1-1.2$ downstream of nappe impact for the duration of the breaker with $d_1=0.4$ m (Fig. 9). Fig. 9 presents time variations of the depth-averaged air content C . Note that one set of data marked ($X=-0.275$) was measured at the rear wall ($x=-0.11$ m, Fig. 2A). Fig. 9 shows that the void fraction was constant in average for the duration of the plunging breaker at a given location. Further, it was found that the water level rise drops near $x=1$ m ($X=2.5$), and a similar observation was made during experiments Series 2.

The results of wave data analysis suggest further that air entrainment affects the wave field, particularly the more energetic waves. Fig. 10 presents a typical FFT analysis conducted on the differential wave signals of two experiments for identical initial conditions with and without air entrainment: i.e., {experiment with air entrainment} – {experiment with plastic sheets} (the time origins were set on the first wave

crest). Fig. 10A shows the energy spectra and Fig. 10B shows the ratio for energy for frequencies between 0.49 and 0.78 Hz to the total wave energy for the experiment with air entrainment. Fig. 10A highlights three dominant frequency ranges: around 0.18 Hz which corresponds to the duration of the pseudo-breaker (about 7–8 s), around 0.5–0.7 Hz and around 2 Hz. In Fig. 10A, the second peak (0.5–0.7 Hz) is observed at each gauge and the writers hypothesise that the corresponding wave period (i.e., about 1.6 s) is close to the average bubble rise time d_1/u_r . That is, Fig. 10A suggests an increase in wave energy in the presence of air entrainment at the pseudo-breaker. Further, the energy ratio for the frequencies between 0.49 and 0.78 Hz decreases with increasing distance from the plunging jet impact (Fig. 10B) and this is consistent with the wave amplitude decay associated with wave propagation, and observed during experiments Series 2.

Note that the writers do not explain the third energy peak around 1.5–2.5 Hz shown in Fig. 10A.

5.2. Saltwater vs. freshwater experiments

While present experiments were conducted with freshwater, seawater has different physical and chemical properties (e.g., Riley and Skirrow, 1965). The difference in physical properties may affect the air entrainment, bubble breakup in the developing flow region and the detrainment rate.

The quantity of entrained air may be estimated using Eq. (2) and a change in inception velocity V_c associated with a change in fluid properties may affect the air entrainment rate. The difference between saltwater and freshwater density and surface tension is about +3% and +1%, respectively, at 20 °C and for 35 ppt salinity (e.g., Chanson et al., 2002). This yields a negligible difference in inception velocity as predicted by Cummings and Chanson (1999) and observed by Chanson et al. (2002).

In turbulent shear flows, a maximum air bubble size D_m may be estimated by the balance between the capillary force and the inertial force caused by the velocity change over distances of the order of the bubble diameter:

$$\frac{\rho_w v^2 D_m}{2\sigma} = (We)_c \tag{7}$$

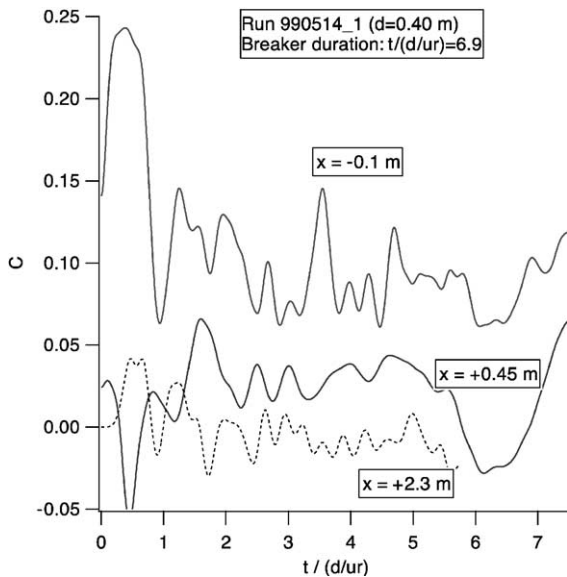


Fig. 9. Fluctuations of the depth-averaged void fraction at three longitudinal locations. $d_1=0.40$ m, Run 990514_1, breaker duration: $6.9d_1/u_r$, $u_r=0.2$ m/s.

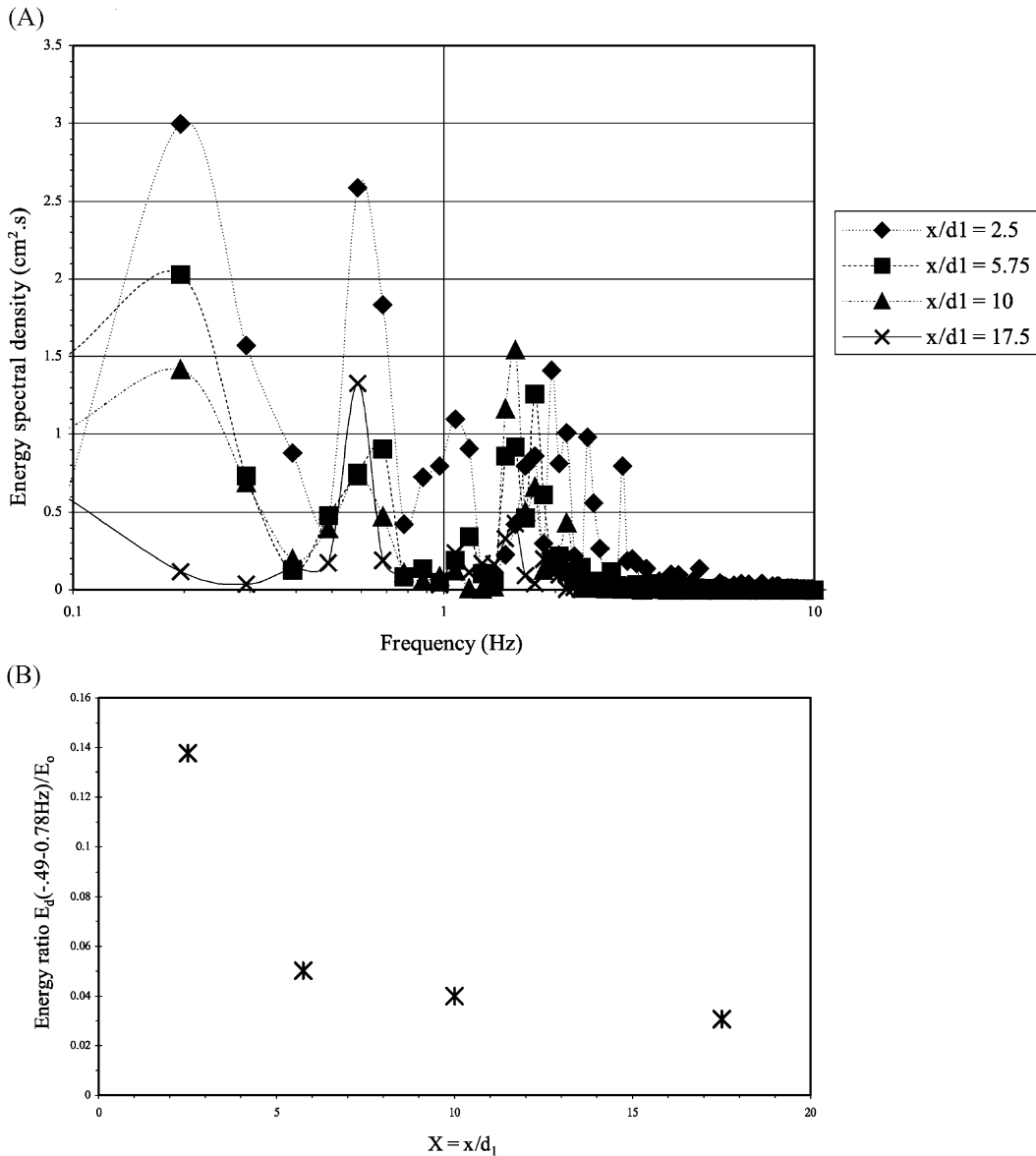


Fig. 10. FFT energy spectral density: {wave data with air entrainment} – {wave data with air entrainment suppression}. $H_1 = 0.57$ m, $d_1 = 0.40$ m—wave gauges: $x = 1, 2.3, 4, 7$ m—{Exp. No. 990514_1} – {Exp. No. 990520-1}. (A) Energy spectral density. (B) Ratio of energy between 0.49 and 0.78 Hz to total wave energy for Exp. No. 990514_1 with air entrainment.

where σ is the surface tension between air and water, v'^2 is the spatial average value of the square of the velocity differences over a distance equal to D_m and $(We)_c$ is the critical Weber number for bubble splitting (Hinze, 1955). Experiments showed that the critical Weber number is a constant near unity (see reviews by

Evans et al., 1992; Chanson, 1995). Eq. (7) implies that the maximum bubble size in saltwater must be about 98% of the maximum size in freshwater shear flows.

For an individual air bubble rising uniformly in a fluid at rest and subjected to a hydrostatic pressure

gradient, the rise velocity depends upon the value of the drag coefficient C_d which is a function of the bubble shape and velocity. Detailed reviews of rise velocity data include Clift et al. (1978) and Comolet (1979). The results suggest little difference in bubble rise velocity between freshwater and saltwater. For small bubbles ($D_{ab} < 0.1$ mm), the rise velocity in saltwater (20 °C, 35 ppt) is about 20% smaller than in freshwater, and the difference tends to be 0 for bubble sizes greater than 1 mm.

Overall, the difference in physical properties between freshwater and saltwater might have little impact on the entrainment rate, bubble breakup and detrainment processes, but the topic requires a detailed comparative study under controlled flow conditions.

6. Summary and conclusions

Physical modelling of a plunging breaker is traditionally conducted according to a Froude similitude. Scale effects may become significant in small-sized models because the breaker duration, bubble rise time and volume of entrained air cannot be properly scaled.

The unsteady air bubble entrainment at a pseudo-plunging breaking wave was physically modelled at near full-scale in the laboratory. Experimental observations highlighted a number of unsteady air–water flow patterns: splashing at jet impact, underwater bubble plume, boiling region next to jet impact. The measurements emphasised high levels of aeration: i.e., depth-average void fraction of more than 10% next to jet impact in shallow waters. The results demonstrated that air entrainment in the surf zone is an important process by inducing a temporary water level rise and modifying the transmitted wave climate, and it cannot be ignored.

Unsteady bubble injection was performed under controlled conditions. The experiments highlighted a very strong vortical motion induced by the rising bubbles. At the start of bubble injection, flow bulking and swarm circulation generated a positive wave propagating along the channel propagating at the celerity of a small disturbance ($\sqrt{gd_1}$). The water level rise (or superelevation) at the origin was associated with a water fall and local high velocities next to the free surface for $X < 1$. At the end of bubble injection, a negative surge propagated in the channel with a rapid decay in circulation.

In summary, the study contributes to a better understanding of unsteady bubble entrainment at a plunging jet and the associated vortical circulation, in part, induced by the rising bubble swarm. But the pseudo-plunging jet had zero horizontal velocity component and model experiments started with the surrounding liquid initially at rest. In the field, plunging breakers are characterised by inclined plunging jets with time-varying jet impact conditions. Wave breaking near the coastline is also associated with significant sediment transport and the resulting flow becomes a three-phase flow: gas (air), liquid (water) and solid (sediment). The challenges ahead of fluid dynamics experts will be to comprehend the interactions between the three phases.

Notation

| | |
|--------------------|---|
| B | channel width (m) |
| C | depth-averaged void fraction or air content |
| d | water depth (m) |
| H | total head (m) above orifice |
| L | length scale (m) |
| L_r | geometric scaling ratio, defined as the ratio of prototype-to-model dimensions |
| Q | water flow rate (m ³ /s) |
| q_{air} | quantity of air entrained at the plunge point (m ² /s) |
| t | time (s) |
| T | dimensionless time: $T = t/(d_1/u_r)$ |
| T_{inj} | dimensionless bubble injection time |
| T_{jet} | dimensionless duration of plunging breaker |
| T_{22} | dimensionless time corresponding to the negative surge generated by end of bubble injection |
| $T_{23\text{max}}$ | dimensionless total duration of water level fluctuations associated with finite duration bubble injection |
| t_{inj} | duration (s) of the air injection |
| t_{jet} | duration (s) of the pseudo breaker |
| u_r | bubble rise velocity (m/s) in still water |
| V | plunging jet velocity (m/s) at nappe impact |
| V_e | onset velocity (m/s) of air bubble entrainment at the plunge point |
| w | vertical plume velocity (m/s) |
| x | horizontal distance (m) |
| X | dimensionless horizontal distance: $X = x/d_1$ |
| y | free-surface elevation (m) measured above the initial still water level |

| | |
|--------------|--|
| Y | dimensionless free-surface elevation measured above still water level: $Y=y/d_1$ |
| $Y_{21\max}$ | dimensionless maximum water elevation following bubble injection |
| $Y_{22\max}$ | dimensionless maximum amplitude of negative surge at end of bubble injection |

Symbols

| | |
|---------------|----------|
| \varnothing | diameter |
|---------------|----------|

Subscript

| | |
|-----|--------------------------------------|
| R | ratio of prototype-to-model quantity |
| 1 | initial flow condition |

Acknowledgements

The authors acknowledge the financial support of the Australian Academy of Science, Japan Society for the Promotion of Science and Ministry of Education, Japan. They further thank the two reviewers, Dr. J. Gemmrich and Dr. H. Oumeraci, for their challenging and constructive comments.

References

- Aoki, S., Chanson, H., Maruyama, M., 2000. Water level rise caused by entrained air bubbles at plunging breakers: an experimental study. Cox, R., Proc. 27th Intl. Conf. Coastal Engineering, Book of Abstracts, Sydney, Australia, July 16–21, vol. 1. Poster 3, 2 pp.
- Bin, A.K., 1993. Gas entrainment by plunging liquid jets. Chem. Eng. Sci. 48 (21), 3585–3630.
- Chanson, H., 1995. Hydraulic Design of Stepped Cascades, Channels, Weirs and Spillways. Pergamon, Oxford, UK January, 292 pp.
- Chanson, H., 1997. Air Bubble Entrainment in Free-Surface Turbulent Shear Flows. Academic Press, London, UK, 401 pp.
- Chanson, H., 1999. The Hydraulics of Open Channel Flows: An Introduction. Butterworth-Heinemann, Oxford, UK, 512 pp.
- Chanson, H., Cummings, P.D., 1994. Effects of plunging breakers on the gas contents in the oceans. Mar. Technol. Soc. J. 28 (3), 22–32.
- Chanson, H., Lee, J.F., 1997. Plunging jet characteristics of plunging breakers. Coast. Eng. 31 (1–4), 125–141, July.
- Chanson, H., Aoki, S., Maruyama, M., 1999. Air bubble entrainment at plunging breakers and its effect on long period waves: an experimental study. Coastal/Ocean Engineering Report, No. COE99-1, Dept. of Architecture and Civil Eng., Toyohashi University of Technology, Japan, July, 41 pp.
- Chanson, H., Aoki, S., Hoque, A., 2002. Similitude of air bubble entrainment and dispersion in vertical circular plunging jet flows. An experimental study with freshwater, salty freshwater and seawater. Coastal/Ocean Engineering Report, No. COE00-1, Dept. of Architecture and Civil Eng., Toyohashi University of Technology, Japan.
- Clift, R., Grace, J.R., Weber, M.E., 1978. Bubbles, Drops, and Particles Academic Press, San Diego, USA, 380 pp.
- Coles, K.A., 1967. Heavy Weather Sailing Adlard Coles, London, UK, 303 pp.
- Comolet, R., 1979. Sur le Mouvement d'une bulle de gaz dans un liquide (Gas bubble motion in a liquid medium). J. Houille Blanche (1), 31–42 (in French).
- Cummings, P.D., Chanson, H., 1999. An experimental study of individual air bubble entrainment at a planar plunging jet. Chem. Eng. Res. Des., Trans. IChemE, Part A 77 (A2), 159–164.
- Daniil, E.I., Gulliver, J., 1991. Influence of waves on air–water gas transfer. ASCE J. Environ. Eng. 117 (5), 522–540.
- Deane, G.B., 1997. Sound generation and air entrainment by breaking waves in the surf zone. J. Acoust. Soc. Am. 102 (5), 2671–2689.
- Evans, G.M., Jameson, G.J., Atkinson, B.W., 1992. Prediction of the bubble size generated by a plunging liquid jet bubble column. Chem. Eng. Sci. 47 (13–14), 3265–3272.
- Fuhrboter, A., 1970. Air entrainment and energy dissipation in breakers. Proc. Int. Conf. Coastal Eng., 391–398.
- Griffin, O.M., 1984. The breaking of ocean surface waves, Naval Research Lab. Memo., Report No. 5337, Washington, USA.
- Henderson, F.M., 1966. Open Channel Flow MacMillan, New York, USA.
- Hinze, J.O., 1955. Fundamentals of the hydrodynamic mechanism of splitting in dispersion processes. AIChE J. 1 (3), 289–295.
- Hughes, S.A., 1993. Physical models and laboratory techniques in coastal engineering. Adv. Ser. Ocean Eng., vol. 7. World Scientific Publishing, Singapore.
- Hwung, H.H., Chyan, J.M., Chung, Y.C., 1992. Energy dissipation and air bubbles mixing inside surf zone. Proc. 23rd Intl. Conf. on Coastal Eng., vol. 1. ASCE, Venice, Italy, pp. 308–321, Chap. 22.
- Ippen, A.T., 1966. Estuary and Coastal Hydrodynamics McGraw-Hill, New York, USA.
- Kanwisher, J., 1963. On the exchange of gases between the atmosphere and the sea. Deep-Sea Res. 10, 195–207.
- Kolovayev, P.A., 1976. Investigation of the concentration and statistical size distribution of wind-producing bubbles in the near-surface ocean layer. Oceanology 15, 659–661.
- Komar, P.D., 1998. Beach Processes and Sedimentation, 2nd edn. Prentice-Hall, Upper Saddle River, NJ, USA, 544 pp.
- Lin, C., Hwung, H.H., 1992. External and internal flow fields of plunging breakers. Exp. Fluids 12, 229–237.
- Longuet-Higgins, M.S., 1988. Mechanisms of wave breaking in deep water. See Surface Sound. In: Kerman, B.R. (Ed.), NATO ASI Series C, vol. 238. Kluwer Academic Publishing, Dordrecht, The Netherlands, pp. 1–30.
- Maruyama, M., 2000. Water level rise and its propagation caused by entrained air bubbles at plunging breakers. Masters thesis, Dept.

- of Architecture and Civil Eng., Toyohashi University of Technology, Japan, 114 pp. (in Japanese).
- Montes, J.S., 1998. *Hydraulics of Open Channel Flow* ASCE Press, New York, USA, 697 pp.
- Nielsen, P., 1984. Field measurements of time-averaged suspended sediment concentrations under waves. *Coast. Eng.* 8, 51–72.
- Perlin, M., He, J., Bernal, L.P., 1996. An experimental study of deep water plunging breakers. *Phys. Fluids* 8 (9), 2365–2374.
- Riley, J.P., Skirrow, G., 1965. *Chemical Oceanography* Academic Press, London, UK, 3 volumes.
- Sawaragi, T., 1995. Coastal engineering—waves, beaches, wave-structure interactions. *Developments in Geotechnical Engineering Series*, vol. 78. Elsevier, Amsterdam, The Netherlands, 479 pp.
- Straub, L.G., Bowers, C.E., Tarapore, Z.S., 1959. Experimental studies of pneumatic and hydraulic breakwaters. Technical Paper No. 25, Series B, St. Anthony Falls Hyd. Lab. University of Minnesota, Minneapolis, USA, 49 pp.
- Thorpe, S.A., 1982. On the clouds of bubbles formed by breaking wind waves in deep water and their role in air–sea gas transfer. *Philos. Trans. R. Soc. Lond., A* 304, 155–210.
- Tulin, M.P., Waseda, T., 1999. Laboratory observations of wave group evolution, including breaking effects. *J. Fluid Mech.* 378, 197–232.
- Wallace, D.W.R., Wirick, C.D., 1992. Large air–sea gas fluxes associated with breaking waves. *Nature* 356, 694–696, 23 April.
- Wood, I.R., 1991. Air entrainment in free-surface flows. *IAHR Hydraulic Structures Design Manual No. 4, Hydraulic Design Considerations*. Balkema, Rotterdam, The Netherlands, 149 pp.